Friction **12**(3): 539–553 (2024)
https://doi.org/10.1007/s40544-023-0794-y
ISSN 2223-7690
CN 10-1237/TH
RESEARCH ARTICLE

Tribological behavior of shape-specific microplate-enriched synovial fluids on a linear two-axis tribometer

Agnese FRAGASSI[1,2], Antonietta GRECO[1], Martina DI FRANCESCO[1], Luca CESERACCIU[3], Aiman ABU AMMAR[4], Israel DVIR[5], Thomas Lee MOORE[1], Haytam KASEM[5,†], Paolo DECUZZI[1,†,*]

[1] *Laboratory of Nanotechnology for Precision Medicine, Fondazione Istituto Italiano di Tecnologia, Genova 16163, Italy*

[2] *Department of Chemistry and Industrial Chemistry, University of Genova, Genoa 16146, Italy*

[3] *Materials Characterization Facility, Istituto Italiano di Tecnologia, Genova 16163, Italy*

[4] *Department of Pharmaceutical Engineering, Azrieli College of Engineering Jerusalem, Jerusalem 9103501, Israel*

[5] *Department of Mechanical Engineering, Azrieli College of Engineering Jerusalem, Jerusalem 9103501, Israel*

Received: 18 June 2023 / Accepted: 02 July 2023

Abstract: Nano- and micro-particles are being increasingly used to tune interfacial frictional properties in diverse applications, from friction modifiers in industrial lubrication to enhanced biological fluids in human osteoarthritic joints. Here, we assessed the tribological properties of a simulated synovial fluid enriched with non-spherical, poly lactic-co-glycolic acid (PLGA) microparticles (μPL) that have been previously demonstrated for the pharmacological management of osteoarthritis (OA). Three different μPL configurations were fabricated presenting a 20 μm × 20 μm square base and a thickness of 5 μm (thin, 5H μPL), 10 μm (10H μPL), and 20 μm (cubical, 20H μPL). After extensive morphological and physicochemical characterizations, the apparent Young's modulus of the μPL was quantified under compressive loading returning an average value of ~ 6 kPa, independently of the particle morphology. Then, using a linear two-axis tribometer, the static (μ_s) and dynamic (μ_d) friction coefficients of the μPL-enriched simulated synovial fluid were determined in terms of particle configuration and concentration, varying from 0 (fluid only) to 6×10^5 μPL/mL. The particle morphology had a modest influence on friction, possibly because the μPL were fully squeezed between two mating surfaces by a 5.8 N normal load realizing boundary-like lubrication conditions. Differently, friction was observed to depend on the dimensionless parameter Ω, defined as the ratio between the total volume of the μPL enriching the simulated synovial fluid and the volume of the fluid itself. Both coefficients of friction were documented to grow with Ω reaching a plateau of $\mu_s \sim 0.4$ and $\mu_d \sim 0.15$, already at $\Omega \sim 2\times10^{-3}$. Future investigations will have to systematically analyze the effect of sliding velocity, normal load, and rigidity of the mating surfaces to elucidate in full the tribological behavior of μPL in the context of osteoarthritis.

Keywords: osteoarthritis; microparticles; tribology; synovial fluid; pin on plate

1 Introduction

Osteoarthritis (OA) is a chronic inflammatory disease of the joints that affects the population across all ages [1]. It is caused by the progressive breakdown of the cartilage and underlying bone, resulting in tissue degeneration, joint pain, limited mobility, and, eventually, permanent disability. Currently, there is no disease-modifying drug capable to reverse the progression of OA and the conventional therapies are mostly palliative, providing only a temporary relief from the symptoms [2–4]. Considering the localized

† Haytam KASEM and Paolo DECUZZI contributed equally to this work.
* Corresponding author: Paolo DECUZZI, E-mail: paolo.decuzzi@iit.it

nature of the disease, the direct injection of therapeutic agents into the joint cavity is a clinically valuable approach, as it avoids possible systemic off-target effects [5, 6]. Usually, treatment options depend on the OA severity and level of pain felt by the patients, where acetaminophen, non-steroidal anti-inflammatory drugs, opioids represent the first line of pharmaceutical intervention [7, 8]. With disease progression, the second option is the intra-articular (IA) injections of corticosteroids, such as dexamethasone, methylprednisolone acetate, triamcinolone acetate, or hyaluronic acid formulations to supplement the viscosity and tribological properties of the synovial fluid (visco-supplementation) [9, 10]. Importantly, the inflammatory component of this disease is associated with the increase in permeability of the blood vessels feeding the joint, inevitably resulting in the rapid clearance of small injected molecules, and even macromolecules like hyaluronic acid [11, 12]. Specifically, extensive experimental investigations have documented that small anti-inflammatory molecules, such as ibuprofen (206.29 Da), diclofenac (296.148 Da), and dexamethasone (392.464 Da) have half-lives in the joints of a few hours, namely 2, 5, and up to 4 h, respectively [13]; while a 3,000 kDa hyaluronic acid is typically associated with an half-life of about 12 h [14].

Given this complex biophysical fingerprint of the disease, the development of drug delivery systems with a sufficiently small size to be intra-articular injected and a sufficiently large size to dwell in the synovial cavity for longer periods of time represents a promising strategy for OA management. Following this line of thought, hydrogels, liposomes, nanoparticles, and microparticles have been investigated as intra-articular drug delivery systems, enabling the release of a variety of molecules over extended periods of time [15–18]. Notably, different studies have confirmed that the dwelling time of drug delivery systems in the synovial cavity depends on their size and materials properties. For instance, Pradal et al. [19] investigated the correlation between particle size and retention time in mouse joints with and without inflammation. Specifically, poly(D, L-lactide) (PLA) nano- and micro-particles, containing fluorescent dyes, were injected in osteoarthritic and healthy mice and particle retention was determined via intravital fluorescence microscopy. Data showed that 300 nm particles spread rapidly out of either inflamed or healthy joints; while micrometric particles were retained for several weeks within the synovial cavity [19]. In another study, Kang et al. [20] confirmed that chitosan nanoparticles exhibited a shorter retention time than microparticles in a OA murine knee joint after intra-articular injection. The authors also confirmed that 20 μm poly lactic-co-glycolic acid (PLGA) particles, tagged with the near infrared fluorescence dye Cy5.5, were retained within a murine osteoarthritic joint for at least 1 month following intra-articular injection [21]. From this evidence, it can be concluded that microparticles are expected to achieve longer intra-articular dwelling times than nanoparticles and, thus, realize sustained drug release to possibly ameliorate joint inflammation and reverse cartilage degeneration. In previous works, the authors have demonstrated the realization of biodegradable microparticles, called microPLates (μPL), made of poly lactic-co-glycolic acid (PLGA) and presenting a 20 μm × 20 μm square base and a tunable height, ranging from 5 μm (thin plates) up to 20 μm (cubic particles). μPL have been loaded with different therapeutic agents, including dexamethasone (DEX) [21], small inhibitors of the CC-chemokine receptor-2 [22]; and ~ 60 nm particles carrying a matrix metalloproteinase 13 (MMP-13) interfering ribonucleic acid (RNA) [23]. In different animal models of osteoarthritis, the authors demonstrated that the sustained release of these therapeutic agents from intra-articularly injected μPL was effective in diminishing joint inflammation and improving overall joint health [21–23]. In this work, a preliminary characterization of the mechanical and tribological properties of these square-shaped μPL with a characteristic height of 5, 10, and 20 μm is provided under different operating conditions. A customized two-axis tribometer was used to measure the static and dynamic friction coefficients of a simulated synovial fluid enriched with μPL, as a function of the particle morphology and concentration.

2 Materials and methods

2.1 Materials

Polydimethylsiloxane (PDMS) (Sylgard 184) and

elastomer were purchased from Dow Corning (Midland, Michigan, USA). Poly(vinyl alcohol) (PVA, Mw 31,000–50,000), poly(D,L-lactide-co-glycolide) (PLGA, lactide:glycolide 50:50, MW 38,000–54,000) and acetonitrile (ACN) were purchased from Sigma-Aldrich (Saint Louis, Missouri, USA). Poly-D-Lysine was purchased from Glibco™-Thermofisher Scientific (Waltham, Massachusetts, USA). Synovial fluid concentrate was purchased from Limb & things (Bristol, UK). Rigid hard counter-face made of a 76 mm × 26 mm × 1 mm soda lime glass plates was purchased from Paul Marienfeld GmbH & Co. KG (Germany).

2.2 Preparation of the PLGA μPL

PLGA μPL were fabricated using a top-down approach as previously reported by the authors [24]**.** Briefly, using a direct laser writing technique, a master template was generated by carving into a silicon wafer a regular matrix of square-shaped wells with an edge size of 20 μm and a depth of 5, 10, or 20 μm. This master template was replicated into a polydimethylsiloxane (PDMS) intermediate template, upon adding a curing agent and baking the whole system in oven at ~ 60 °C for 8 h. Then, the PDMS template was peeled off from the silicon master and a PVA solution (10 w/v % in deionized (DI) water) was deposited over it to obtain, upon exsiccation, a sacrificial PVA template presenting the same regular matrix of well as per the original master template. Finally, a PLGA solutions was spread over the PVA template to carefully fill the wells. After solvent evaporation and PLGA matrix solidification, the so-loaded PVA template was dissolved in DI water at room temperature in an ultrasonic bath. The PVA solution was removed through a polycarbonate membrane filters (40 μm pore size) and the μPL were recovered after two centrifugation steps (1,717×g for 5 min) and stored at 4 °C. Note that, depending on the particle size (i.e., depth of the wells), different amounts of PLGA were dissolved in different volumes of acetonitrile (ACN). Specifically, the 5H and 10H μPL were realized using 10 and 15 mg of PLGA dissolved in a 62.5 μL solution of ACN; whereas the 20H μPL were realized using 60 mg of PLGA dissolved in a 200 μL solution of ACN. Indeed, taller μPL have larger volumes and require a larger mass of polymer.

2.3 Physico-chemical characterization of the PLGA μPL

The physico-chemical characterization of μPL was performed using different, complementary techniques. Specifically, the μPL morphology (shape and size) were observed by using a scanning electron microscope (SEM, Elios Nanolab 650, FEI). Briefly, a drop of sample was spotted on a silicon template and uniformly sputtered with gold to increase the contrast and reduce the sample damaging. An acceleration voltage of 5–15 keV was used for SEM imaging. Moreover, the size distribution and the number of μPL were evaluated via a Multisizer 4 COULTER particle counter (Beckman Coulter, CA).

2.4 Mechanical characterization of the PLGA μPL

The mechanical properties of the PLGA μPL were investigated via nanoindentation using a Chiaro nanoindenter (Optics 11 Life). This device uses a piezo-driven actuator to apply controlled indentation to the samples, while evaluating the reaction force from deflection of a cantilever probe, measured by interferometry. The system was equipped with a spherical probe with 9 μm diameter and a cantilever with a stiffness of 4 N/m. Tests were conducted under DI water inside a glass petri dish, previously coated with poly-D-lysine to promote the attachment of the particles to the substrate. μPL were identified individually through an inversed microscope coupled with the nano-indenter and indented in displacement control, at a rate of 4 μm/s, over the particle core to avoid any border effect. Typical indentations reached a maximum load of 20–40 μN and penetration depth of ~400 nm. After testing, the load–indentation (force–penetration) curves were fitted with the classical Hertz equation to extract the apparent Young's modulus under compression loading. From the slope of the force–displacement curves, the Young's modulus Y was calculated through the classical Hertzian equation $F = 2RYh$, where F is the applied force, h is the tip displacement, R is the tip radius. To reduce the influence of the substrate on the measurements, the force–displacement curve fitting was limited to

the initial loading portion, up to 30% of the maximum load. Only indentations with a fitting coefficient $R^2 > 0.9$ were selected and at least 10 particles per conditions were considered.

2.5 Customized two-axis tribometer

The tribological behavior of the PLGA μPL was investigated using a customized two-axis tribometer designed and constructed in the Tribology Laboratory at the Azrieli College of Engineering in Jerusalem [25]. Based on a moving horizontal counter-face, this device allows one to evaluate the tribological properties (friction, adhesion, and peeling) of different materials, including textured surfaces, under dry or wet contact conditions according to needs. In this tribometer, the drive unit consisted of three translation stages (two motorized and one manual) to adjust the contact location and apply the loads between the friction pair components. In the present study, the friction pair consisted of a Teflon upper disk (a cylinder of 10 mm height and 10 mm diameter, cut directly from a Teflon rod) mounted on the tribometer via a self-alignment system, and a bottom glass counter surface. On the bottom glass, 500 μL of simulated synovial fluid (SF) enriched with different amount of PLGA μPL were deposited, prior to each test or repetition, to conduct the friction tests under lubricated contact condition. The measurement unit consisted of two load cells (FUTEK's FSH00092-LSB200) to measure force variations with a high resolution (0.1 mN) both in the normal and tangential directions. The operating and control software were written in a LabVIEW environment. The measurements were sampled with a multifunctional data acquisition board Lab-PC-NI USB-6211 (National Instruments Co., Austin, Texas, USA) and processed using a LabVIEW 2017 software package (National Instruments Corporation, 11,500 N. Mopac Expressway, Austin, Texas, 78759, USA). The current study used a passive self-aligning system to ensure full flat-on-flat contact between the mating surfaces during the entire friction test.

2.6 Experimental determination of the friction coefficients

All experiments were performed at the room temperature of 25 ± 1 °C and under a relative humidity of 35% ± 5%. As surface roughness plays a significant role in determining the frictional properties, in this study, prior to each friction tests, a controlled polishing process was used to obtain high surface finish of the mating surfaces. Specifically, surface polishing was achieved by gradually decreasing in stages of 120, 320, 500, and 1,000 to 1,200 grit. Then, after the polishing, all the samples were characterized using an optical profilometer (NT1100, Wyko, USA) to evaluate the surface roughness of the surfaces. The arithmetic average roughness R_a was reduced from R_a ~ 900 nm before polishing to 240–260 nm. The glass counterface (76 mm × 26 mm × 1 mm) was cleaned with ethanol. Then, the Teflon rod and glass substrate were mounted on the tribometer, and the glass counter-face was covered with 500 μL of simulated synovial fluid, either blank or enriched with PLGA μPL. A single friction cycle consisted of 8 consecutive steps: (i) approaching: the glass counter-face is moved up in the vertical direction and brought into contact with the Teflon rod, leading to a gradual increase in the normal load P until the desired predefined value of 5.8 N is reached; (ii) waiting: the system is left to accommodate for 0.5 s; (iii) tangential movement: the Teflon rod is moved in the tangential direction at a constant sliding velocity of 1 mm·s^{-1} for a total crossed distance of 20 mm. During this step, the normal load is fixed, while the tangential force resisting the sample motion is recorded; (iv) waiting: the system is left to accommodate for 0.5 s; (v) disconnecting: the glass counter-face is withdrawn in the vertical opposite direction until a complete separation of the mating surfaces is achieved; (vi) waiting: the system is left to accommodate for 0.5 s; (vii) back to the starting point: the stage holding the glass counter-face is moved back to its initial position. Importantly, the contact is open during steps (vi) and (vii) allowing the working solution to fully cover the frictional surface; (viii) waiting: the system is left to accommodate for 0.5 s. At this point, a new test cycle can start.

During each test cycle, the static friction coefficient μ_s was computed by dividing the max tangential force measured at the sliding inception point by the applied normal force ($\mu_s = F_s/P$), while the dynamic friction coefficient μ_d was computed as the average friction force measured in the stabilized zone (middle

of the sliding stock) divided by the applied normal force ($\mu_d = <F_d>/P$)). In the present study, the influence of the PLGA μPL on the friction coefficient was evaluated by suspending various aliquots of microparticles in the simulated synovial fluid, placed at the interface between the friction pair. Each run consisted of 13 friction cycles performed consecutively: the first 3 cycles were considered as running-in without recording, while the following 10 cycles were recorded and saved to be analyzed and estimate the friction coefficients. Upon completion of the 13th cycle, the 500 μL solution was removed using Kimwipes before starting the subsequent run. Each PLGA μPL configuration (5H, 10H, and 20H PLGA μPL) was tested 3 times using a new friction pair (Teflon and glass counter face) for each repetition.

3 Results

3.1 Fabrication and physical-chemical characterization of PLGA μPL

Three configurations of PLGA μPL were synthesized following a multi-step, top-down fabrication process (Fig. 1(a)), previously described by the authors [21]. In brief, a regular array of 20 μm × 20 μm squared wells was carved into a silicon template using a laser writing technique. This master template was then replicated into an intermediate PDMS template and a final, sacrificial PVA template presenting the same array of squared wells as in the silicon master template. The depth of the wells was defined to be 5, 10, or 20 μm, leading to three different microparticles. Finally, a PLGA solution was uniformly spread on

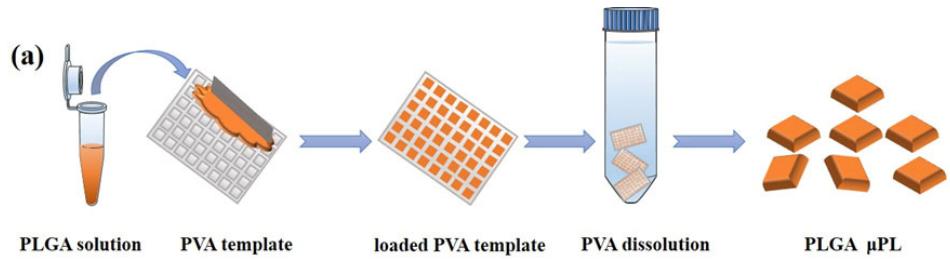

(b)

μPL	Base size (μm)	Height (μm)	PLGA (mg)	ζ- Pot (mV)
5H	20x20	5	10	-24.0 ± 3.3
10H	20x20	10	15	-25.8 ± 2.6
20H	20x20	20	60	-24.2 ± 2.7

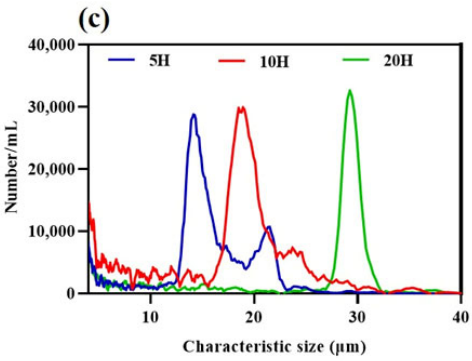

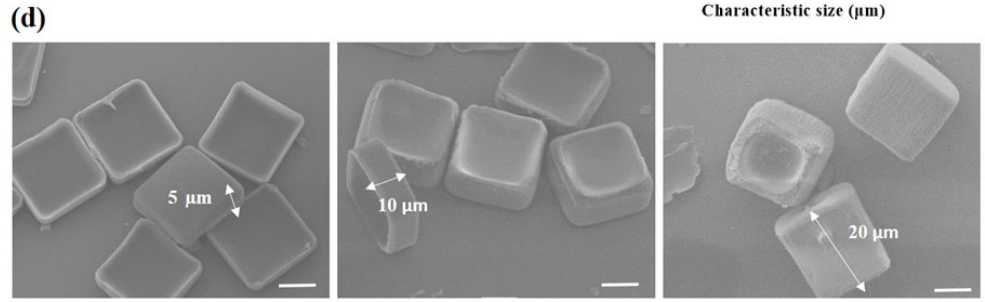

Fig. 1 Morphological and physico-chemical characterization of PLGA μPL. (a) Schematic representation of the top-down fabrication process for the shape-specific PLGA μPL; (b) three μPL configurations presenting different heights, namely 5 μm (5H), 10 μm (10H), and 20 μm (20H); PLGA amounts; and surface electrostatic ζ-potential. All the μPL configurations have a square base with an edge size length of 20 μm; (c) multisizer coulter counter size distribution profiles for the three μPL configurations; and (d) SEM images documenting the different height for the three μPL configurations (scale bar: 10 μm).

the PVA template to carefully fill up all the wells. By changing the depth of the wells and the amount of PLGA, μPL with a height of 5 μm (5H μPL), 10 μm (10H μPL), and 20 μm (20H μPL) were realized, as listed in Fig. 1(b). Notice that the amounts of PLGA used for fabricating the μPL were progressively increased with the particle height in order to properly fill the wells in the sacrificial PVA template. All μPL configurations were characterized by scanning electron microscopy (SEM) and multisizer coulter counter (Figs. 1(c) and 1(d)). SEM analyses showed that the size and shape of the microparticles accurately matched those of the wells in the original silicon templates. In particular, the SEM images of Fig. 1(d) show a well-defined μPL morphology with a common edge size length of 20 μm and heights of 5, 10, and 20 μm. A modest concavity of the particle surface is also observed, resulting from the loading process. The difference in size among the three configurations were further confirmed via multisizer coulter counter analysis that showed single peaks around 15, 20, and 30 μm for the 5H, 10H, and 20H μPL, respectively (Fig. 1(c)). Notice that the thinnest particles with a height of 5 μm are associated with a size distribution presenting two peaks: a major peak at 15 μm and a minor peak around 20 μm. The tallest peak derives from the average between the edge size length (20 μm) and the nominal height (5 μm) of the 5H μPL. The secondary peak tends to disappear with the 10H μPL, who have a major peak around the edge size length (20 μm). For the 20H μPL, the secondary peak is absent and only a single peak is visible at 30 μm. It is here important to highlight that a Multisizer system estimates size distributions assuming that the particles are spherical and cannot be considered as an absolute measurement of the size for non-spherical particles, thus explaining the apparent deviation between the SEM and the Multisizer peak measurements.

3.2 Mechanical characterization of PLGA μPL

Then, nanoindentation experiments were conducted to assess the apparent Young's modulus under compressive loading of the three μPL configurations, using a commercially available nanoindenter (Fig. 2(a)). Following the described protocols, load–indentation curves were obtained for all three μPL configurations. A representative curve is provided in Fig. 2(b), showing a loading phase till a maximum penetration depth of ~ 600 nm, followed by a holding phase around 30–35 μN, and an unloading phase down to eventually 0 μN. At least 10 similar load–indentation curves were generated for each of the three μPL configurations. Then, these curves were fitted with the classical Hertz theory equation to extract the Young's modulus of the indented particles considering only the loading phase up to a penetration depth of 400 nm (dashed green line, Fig. 2(b)), in order to minimize any possible effect associated with the substrate rigidity. Notice that the thinnest particle had a thickness of 5 μm, which is more than 10 times larger than the reference penetration depth of 400 nm. The Young's moduli for the three μPL configurations are listed in Fig. 2(c), presenting values of 5.7 ± 2.4, 5.9 ± 2.9, and 5.1 ± 3.1 MPa for the 5H, 10H, and 20H μPL, respectively. No statistically significant difference was detected among the three μPL configurations (Fig. S1 in the Electronic Supplementary Material (ESM)). This analysis demonstrates that the elastic response of the μPL, under compression, is independent of their thickness, at least for the particle size range considered in the present study.

3.3 Tribological characterization of PLGA μPL

The tribological properties of the μPL were evaluated on a customized two-axis tribometer, designed, and constructed in the Tribology Laboratory at the Azrieli College of Engineering in Jerusalem [25]. Figure 3(a) shows a schematic representation of the device that includes two main units, one for driving and operating the system, and one for measuring all the relevant forces. The driving unit comprises three translation stages to adjust the contact location and apply loads between a 10 mm Teflon cylinder and a glass counter surface. The tribological properties of the simulated synovial fluid (SF), without or enriched with PLGA μPL, were analyzed by depositing the working solution on the counter glass surface and operating the device following 8 specific steps, as pictured in Fig. 3(b) and described in Section 2. By measuring the tangential forces in step 3, upon pushing the counter glass surface against the Teflon rod with a normal load $P = 5.8$ N (apparent contact

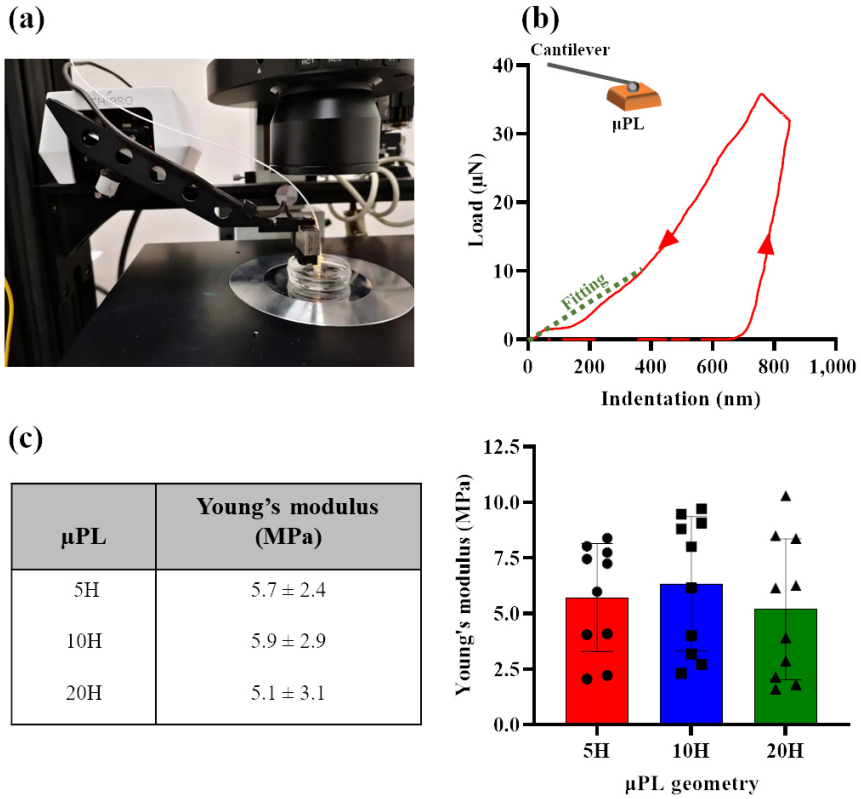

μPL	Young's modulus (MPa)
5H	5.7 ± 2.4
10H	5.9 ± 2.9
20H	5.1 ± 3.1

Fig. 2 Mechanical characterizations of PLGA μPL. (a) Image depicting the stage and loading beam of a Chiaro nanoindenter (Optics 11 Life) equipped with a 9 μm spherical tip; (b) a representative load–indentation curve. Following the curve in a clock-wise direction, it comprises a loading phase till a maximum depth of ~ 400 nm, a holding phase at around 30–35 μN, and an unloading phase down to 0 μN. The apparent Young's modulus is estimated by fitting the loading portion of the indentation curves using the conventional Hertz theory (green dashed line); and (c) apparent Young's modulus for three different μPL configurations, presenting a height of 5 μm (5H), 10 μm (10H), and 20 μm (20H) (n = 10).

pressure of 68 kPa) and sliding it over a 20 mm distance with a speed of 1 mm·s^{-1}, the characteristic friction coefficient curves can be generated under different experimental conditions (Fig. 3(c)). Specifically, the static friction coefficient μ_s is related to the inception point ($\mu_s = F_s/P$) while the dynamic friction coefficient μ_d is related to the 'stabilized zone' ($\mu_d = \langle F_d \rangle/P$). No microparticles were observed to adhere at the Teflon surface post testing (Fig. S2 in the ESM).

The PLGA μPL were resuspended in simulated synovial fluid at various concentrations, for each of the three morphological configurations. The tribological performance of the resulting particle-enriched simulated synovial fluid was characterized in terms of static and dynamic friction coefficients. Figure 4(a) shows the typical friction coefficient curves for the three different particle geometries, namely 5H, 10H, and 20H μPL, and four different concentrations, namely 0.6 × 10^5, 1.2 × 10^5, 6 × 10^5, and 0 μPL/mL, which corresponds to the native simulated synovial fluid with no particles. Although the friction curves present similar trends, clearly documenting a peak (static friction coefficient μ_s) followed by a stable phase (dynamic friction coefficient μ_d), the values of the coefficients of friction are strongly affected by the presence of the μPL. This is more clearly documented by the bars in the chart of Fig. 4(b). At sufficiently low particle concentrations (< 0.6 × 10^5 μPL/mL), no statistically significant difference is observed for the friction coefficients between the native and the μPL-enriched synovial fluids. However, as the μPL concentration increases, both the static and dynamic coefficient of friction increase too reaching values as high as μ_s ~ 0.4 and μ_d ~ 0.2 at 6 × 10^5 μPL/mL. The increase in friction coefficients appears to be associated with the piling up of microparticles at the leading edge of the sliding pair as the μPL concentration increases (Fig. S3 in the ESM). Differently, for a fixed

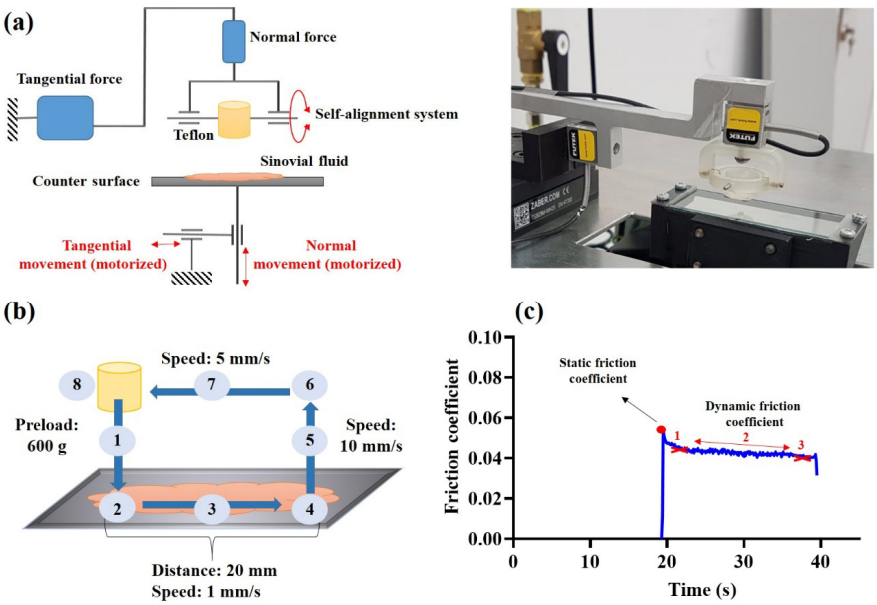

Fig. 3 Tribological apparatus and operation. (a) Schematic representations (left) and image (right) of a customized linear two-axis tribometer used for the tribological characterizations. The apparatus consists of tangential and normal force load cells, a friction pair comprising a 10 mm Teflon rod, with its self-alignment system, and a counter glass surface with a rubber belt to retain the working fluid; (b) the apparatus is operated following a cycle of 8 consecutive steps, including the sliding phase 3 during which tangential forces are continuously measured under a fixe normal load (5.8 N); and (c) a representative curve showing the typical variation of the friction coefficient during the sliding step. The static coefficient of friction is calculated at the onset of sliding (red dot – {1}), whereas the dynamic coefficient of friction is calculated by averaging the tangential force during the stable sliding phase (red double edge arrow – {2}).

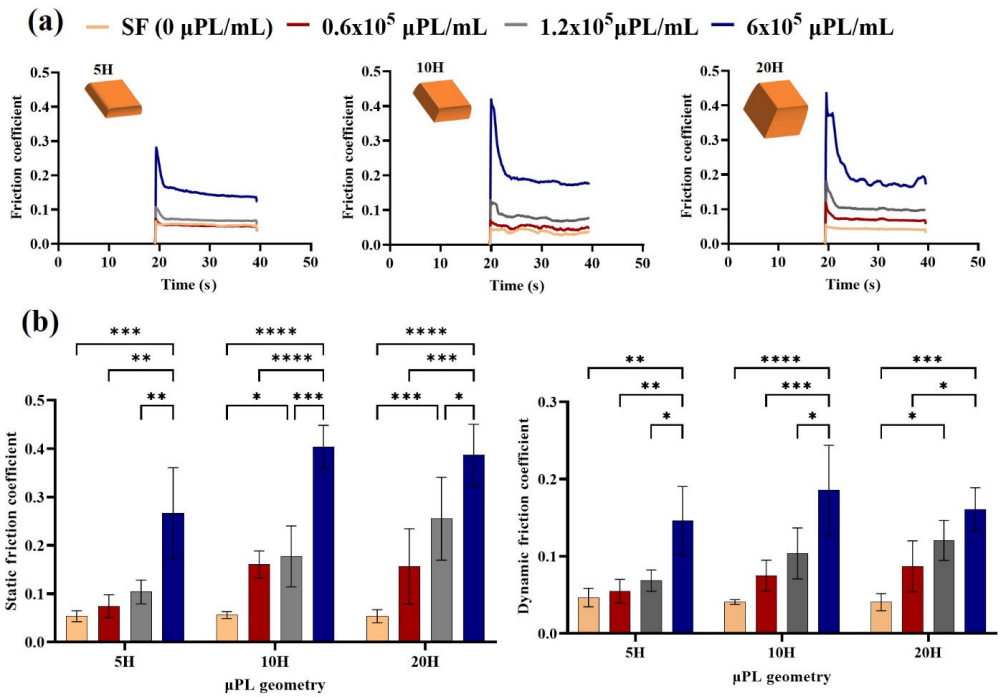

Fig. 4 Static and dynamic coefficients of friction of PLGA µPL. (a) Representative curves for the coefficients of friction of 5 µm (5H µPL), 10 µm (10H µPL), and 20 µm (20H µPL) tall µPL dispersed in simulated synovial fluid at different concentrations (SF alone–red line; 0.6×10^5 µPL/mL–brown line; 1.2×10^5 µPL/mL–gray line; 6×10^5 µPL/mL–blue line); (b) static (left) and dynamic (right) coefficients of friction for various µPL morphology and concentrations ($n \geq 30$; *: $p < 0.05$; **: $p < 0.01$; ***: $p < 0.005$; ****: $p < 0.001$). Data presented as average ± standard deviation.

particle concentration (same color bars), the variations in static and dynamic coefficients of friction are modest and statistically less relevant.

Based on this observation, the total volumetric particle concentration Ω was introduced as the ratio between the total volume of the microparticles and the volume of the solution in which they are dispersed. Therefore, if n is the number of microparticles and $V_p = 400H$ μm^3 is the volume of a single microparticle with edge side length of 20 μm and a height H (in μm), the dimensionless volumetric particle concentration Ω takes the form:

$$\Omega = \frac{nV_p}{V_s} = 8nH \times 10^{-10}$$

where V_s is the volume of the simulated synovial fluid (500 μL = 5×10^{11} μm^3). Indeed, for the native synovial fluid without microparticles enrichment, Ω is equal to zero. As the particle concentration in solution increases, the value of Ω increases linearly too. Importantly, Ω does not take into consideration the microparticle morphology but only its concentration. In Fig. 5(a), the static and dynamic friction coefficients for the three μPL configurations have been reorganized and presented for fixed Ω values. The differently colored bars are therefore related to experiments conducted with different μPL (5H: red bars; 10H: blue bars; and 20H: green bars) at the same Ω concentrations. Notably, no statistically significant difference is observed among the three particle configurations for a given Ω (Fig. S4 in the ESM). This would confirm what already observed in Fig. 4(b), that both friction coefficients depend mostly on the particle concentration Ω rather than the particle morphology. Moreover, by plotting the friction coefficient as a function of Ω (Fig. 4(b)), it could be inferred that both coefficients tend to a plateau for sufficiently high values of Ω. Specifically, for $\Omega > 2 \times 10^{-3}$, μ_s and μ_d would tend to ~ 0.4 and ~ 0.15, respectively. Finally, upon reorganizing the same data in a semi-logarithm plot (Fig. 5(c)), it can be inferred that the friction coefficients grow quasi logarithmically

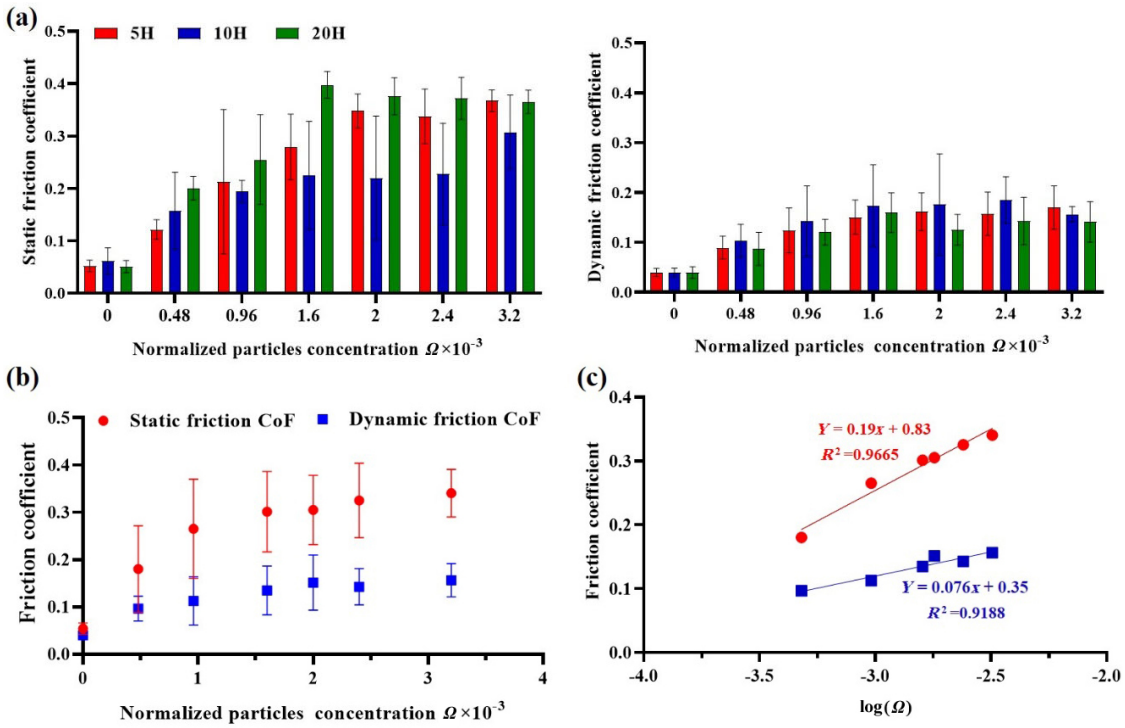

Fig. 5 Coefficients of friction of the PLGA microplates as a function of the normalized concentration Ω. (a) Static (left) and dynamic (right) coefficients of friction as a function of the normalized concentration Ω and for different μPL configurations; (b) static (red line) and dynamic (blue line) coefficients of friction as a function of the normalized concentration Ω plateauing already at $\Omega \sim 2 \times 10^{-3}$; and (c) static (red line) and dynamic (blue line) coefficients of friction as a function of the normalized concentration Ω in a semi-logarithm diagram and corresponding interpolating expressions.

with the volumetric particle concentration Ω following the relations:

$$\mu_s \approx 0.19 \cdot \log\Omega + 0.83 \text{ with } R^2 = 0.9665$$

$$\mu_d \approx 0.076 \cdot \log\Omega + 0.35 \text{ with } R^2 = 0.9188$$

4 Discussion

Multiple experimental evidence, from the authors and other laboratories, have shown that intra-articularly injected microparticles have longer dwelling times than small molecules, macromolecules, and nanoparticles in both healthy and osteoarthritic joints [13, 14]. This is essentially due to the slower, or even impaired, filtration of such larger constructs across the hyperpermeable walls of the synovium in the inflamed joint [26]. Also, microparticles can carry larger amounts of therapeutic agents and release them over the course of several weeks, as opposed to nanoparticles that would instead require multiple consecutive injections to achieve comparable drug dosing. Moreover, it should be kept in mind that, microparticles have a characteristic size comparable to that of most cells populating the joint, including chondrocytes and synovial macrophages. As such, in addition to their pharmacological activity, microparticles could provide a mechanical function upon intra-articular deposition. Indeed, previous data from the authors have shown μPL to distribute within the synovial cavity and align at the cartilage/synovial fluid interface, where they could function as microscopic cushions [21].

This was the main motive for assessing the tribomechanical properties of polymeric microparticles presenting different morphologies, ranging from thin platelets (5H μPL) to cubical particles (20H μPL), and made of PLGA, being one of the most extensively used polymers in biomedical applications. This study showed that, for sufficiently low particle concentrations (< 100,000 μPL/ml, or $\Omega < 0.5 \times 10^{-3}$), the simulated synovial fluid enriched with μPL has tribological properties comparable to that of the native lubricant, regardless of the particle morphology. However, at higher particle concentrations (> 100,000 μPL/ml, or $\Omega > 0.5 \times 10^{-3}$), both the static and dynamic coefficients of friction of the enriched synovial fluid increase with Ω reaching values up to 8 and 3 times higher than the native fluid, respectively.

It is here important to recall that the modulation of interfacial friction by particle-enriched lubricants is governed by different mechanisms and depends on the morphological and mechanical properties of the mating surfaces and particles [27]. On rough surfaces, sufficiently small particles would fill the superficial irregularities originating a flatter and more uniform sliding interface. Under this condition, a minimum in friction is typically achieved for an optimal particle concentration: at low concentrations, the number of added particles is not sufficient to 'regularize' the sliding interface; at high concentrations, the excess of particles tends to form clusters that impair sliding. Differently, on smooth surfaces, sufficiently stiff particles could act as balls in rolling bearings and transform sliding into rolling friction [28]; whereas deformable particles would squeeze or even exfoliate under tangential loading and form a film at the interface [29].

In the current configuration, the working fluid enriched with μPL was trapped between a 10 mm Teflon rod and a glass countersurface, pushed together by a total compressive load of 5.8 N. The surfaces were polished to have a roughness $R_a \sim 250$ nm, which is much smaller than the micrometric size of μPL. Also, given the geometry and deformability of μPL as compared to the rigid mating surfaces, these microparticles cannot operate as rolling elements. Consequently, assuming the total normal load (P = 5.8 N) being equally distributed over 10^6 particles with a A = 20 μm × 20 μm cross section and a E = 6 kPa Young's modulus, the 5H, 10H, and 20H μPL would be fully squeezed at the interface by ~12, 24, and 48 μm, respectively ($=10^{-6} \cdot PH/(EA)$). Indeed, this is a conservative estimate, as part of the load P would be distributed over the sub-micrometric asperities of the two mating surfaces. However, it does suggest that, under the actual testing conditions, μPL would be fully squeezed, regardless of their original morphology. Another important factor to consider is the spatial distribution of the μPL at the sliding interface. Indeed, 10^6 μPL tightly sitting next to each other on the glass countersurface would cover an area of 4 cm^2 which is 5 times larger than the base area of the 10 mm

Teflon rod (0.785 cm^2). Thus, it is likely that, as the number of particles grows beyond 10^6, some of them would either escape from the contact area or pile up to form multiple layers. Indeed, during the experiments, a larger concentration of PLGA μPL was observed accumulating at the leading edge of the sliding pair. This build-up of microparticles at the sliding front could explain the increase in friction with Ω.

Based on the above reasonings, future studies on the tribological performance of μPL-enriched fluids should address some limitations of the present study. First, the normal load P and sliding velocity should be adjusted to reproduce different loading and kinematic conditions, reaching contact pressures as high as a few MPa [30]. Second, the mating surfaces should be realized with soft materials or, at least, one of the surfaces should be similar to articular cartilage. Given the biological complexity and architecture of cartilage, it is not surprising that several studies have documented major discrepancies in friction coefficients depending on the nature of the sliding pairs and interposed fluid [31, 32].

5 Conclusions

Three configurations of poly lactic-co-glycolic acid (PLGA) microparticles (μPL) were fabricated with the same square base of 20 μm × 20 μm and a height ranging from very thin (5 μm) to cubical (20 μm) particles. No statistically significant differences in physico-chemical and mechanical properties were documented for the three configurations, returning a surface electrostatic ζ potential of –25 mV and a compressive Young's modulus of ~6 kPa. The tribological properties of the PLGA μPL resuspended in simulated synovial fluid were characterized using a customized two-axis tribometer quantifying the static and dynamic coefficients of friction as a function of the particle morphology and volumetric concentrations. Under boundary-like lubrication, the static and dynamic coefficients of friction were documented to increase rapidly with the particle concentration up to a plateau of ~ 0.4 and ~ 0.15, respectively. Given the full compression of the particle between the two mating surfaces, the morphology of the PLGA μPL had only a modest effect on the friction coefficients. Additional work will have to be performed in the future to fully characterize the tribological behavior of these PLGA microparticles by varying systematically the sliding speed, normal load, and rigidity of the mating surfaces.

Acknowledgements

Agnese FRAGASSI (A.F.) and Paolo DECUZZI (P.D.) acknowledge the partial support of the Horizon 2020 Marie Skłodowska-Curie Actions project "Shaping the Mechano-Pharmacological properties of Microparticles and Extracellular Vesicles for the Treatment of Osteoarthritis–MEPHOS" with Grant agreement 872648. A.F. acknowledges the support of the Internationalization Program of the Jerusalem College of Engineering (JCE) for conducting research activities in the laboratories of Profs. Haytam KASEM and Aiman ABU AMMAR.

Declaration of competing interest

The authors have no competing interests to declare that are relevant to the content of this article.

Electronic Supplementary Material: Supplementary material is available in the online version of this article at https://doi.org/10.1007//s40544-023-0794-y.

References

[1] Loeser R F, Collins J A, Diekman B O. Ageing and the pathogenesis of osteoarthritis. *Nat Rev Rheumatol* **12**: 412–420 (2016)

[2] Martel-Pelletier J, Barr A, Cicuttini F, Conaghan P, Cooper C, Goldring M, Goldring S R, Jones G, Teichtahl A J, Pelletier J P. Osteoarthritis. *Nat Rev Dis Primers* **2**: 16072 (2016)

[3] Menon J, Mishra P. Health care resource use, health care expenditures and absenteeism costs associated with osteoarthritis in US healthcare system. *Osteoarthr Cartilage* **26**: 480–484 (2018)

[4] Turkiewicz A, Petersson I F, Björk J, Hawker G, Dahlberg L E, Lohmander L S, Englund M. Current and future impact of osteoarthritis on health care: A population-based study with projections to year 2032. *Osteoarthr Cartilage* **22**: 1826–1832 (2014)

[5] Evans C H, Kraus V B, Setton L A. Progress in intra-articular therapy. *Nat Rev Rheumatol* **10**: 11–22 (2014)

[6] Jones I A, Togashi R, Wilson M L, Heckmann N, Vangsness Jr C T. Intra-articular treatment options for knee osteoarthritis. *Nat Rev Rheumatol* **15**: 77–90 (2019)

[7] Kolasinski S L, Neogi T, Hochberg M C, Oatis C, Guyatt G, Block J, Callahan L, Copenhaver C, Dodge C, Felson D, et al. 2019 American college of Rheumatology/Arthritis foundation guideline for the management of osteoarthritis of the hand, hip, and knee. *Arthritis Rheumatol* **72**: 220–233 (2020)

[8] Bannuru R R, Osani M, Vaysbrot E, Arden N, Bennell K, Bierma-Zeinstra S, Kraus V B, Lohmander L S, Abbott J H, Bhandari M, et al. OARSI guidelines for the non-surgical management of knee, hip, and polyarticular osteoarthritis. *Osteoarthr Cartilage* **27**: 1578–1589 (2019)

[9] Hepper C T, Halvorson J J, Duncan S T, Gregory A J, Dunn W R, Spindler K P. The efficacy and duration of intra-articular corticosteroid injection for knee osteoarthritis: A systematic review of level I studies. *J Am Acad Orthop Sur* **17**: 638–646 (2009)

[10] Bannuru R R, Natov N S, Obadan I E, Price L L, Schmid C H, McAlindon T E. Therapeutic trajectory of hyaluronic acid versus corticosteroids in the treatment of knee osteoarthritis: A systematic review and meta-analysis. *Arthrit Care Res* **61**: 1704–1711 (2009)

[11] Wehling P, Evans C, Wehling J, Maixner W. Effectiveness of intra-articular therapies in osteoarthritis: A literature review. *Ther adv musculoskel* **9**: 183–196 (2017)

[12] Brown S, Kumar S, Sharma B. Intra-articular targeting of nanomaterials for the treatment of osteoarthritis. *Acta Biomater* **93**: 239–257 (2019)

[13] Larsen C, Østergaard J, Larsen S W, Jensen H, Jacobsen S, Lindegaard C, Andersen P H. Intra-articular depot formulation principles: Role in the management of postoperative pain and arthritic disorders. *J Pharm Sci* **97**: 4622–4654 (2008)

[14] Maudens P, Jordan O, Allémann E. Recent advances in intra-articular drug delivery systems for osteoarthritis therapy. *Drug Discovery Today* **23**: 1761–1775 (2018)

[15] Dong J, Jiang D, Wang Z, Wu G, Miao L, Huang L. Intra-articular delivery of liposomal celecoxib–hyaluronate combination for the treatment of osteoarthritis in rabbit model. *Int J Pharm* **441**: 285–290 (2013)

[16] Bedingfield S K, Colazo J M, Yu F, Liu D D, Jackson M A, Himmel L E, Cho H, Crofford L J, Hasty K, Duvall C L. Amelioration of post-traumatic osteoarthritis via nanoparticle depots delivering small interfering RNA to damaged cartilage. *Nature Biomed Eng* **5**: 1069–1083 (2021)

[17] Bodick N, Lufkin J, Willwerth C, Kumar A, Bolognese J, Schoonmaker C, Ballal R, Hunter D, Clayman M. An intra-articular, extended-release formulation of triamcinolone acetonide prolongs and amplifies analgesic effect in patients with osteoarthritis of the knee: A randomized clinical trial. *J Bone Joint Surg Am* **97**: 877–888 (2015)

[18] Di Francesco M, Fragassi A, Pannuzzo M, Ferreira M, Brahmachari S, Decuzzi P. Management of osteoarthritis: From drug molecules to nano/micromedicines. *Wiley Interdiscip Rev Nanomed Nanobiotechnol* **14**: e1780 (2022)

[19] Pradal J, Maudens P, Gabay C, Seemayer C A, Jordan O, Allémann E. Effect of particle size on the biodistribution of nano-and microparticles following intra-articular injection in mice. *Int J Pharm* **498**: 119–129 (2016)

[20] Kang M L, Ko J Y, Kim J E, Im G I. Intra-articular delivery of kartogenin-conjugated chitosan nano/microparticles for cartilage regeneration. *Biomaterials* **35**: 9984–9994 (2014)

[21] Di Francesco M, Bedingfield S K, Di Francesco V, Colazo J M, Yu F, Ceseracciu L, Bellotti E, Di Mascolo D, Ferreira M, Himmel L E, et al. Shape-defined microplates for the sustained intra-articular release of dexamethasone in the management of overload-induced osteoarthritis. *ACS Appl Mater Interfaces* **13**: 31379–31392 (2021)

[22] Ozkan H, Di Francesco M, Willcockson H, Valdés-Fernández J, Di Francesco V, Granero-Moltó F, Prosper F, Decuzzi P, Longobardi L. Sustained inhibition of CC-chemokine receptor-2 via intraarticular deposition of polymeric microplates in post-traumatic osteoarthritis. *Drug Delivery Transl Res* **13**: 689–701 (2023)

[23] Bedingfield S K, Colazo J M, Di Francesco M, Yu F, Liu D D, Di Francesco V, Himmel L E, Gupta M K, Cho H, Hasty K A, et al. Top-down fabricated microplates for prolonged,

intra-articular matrix metalloproteinase 13 siRNA nanocarrier delivery to reduce post-traumatic osteoarthritis. *ACS Nano* **15**: 14475–14491 (2021)

[24] Di Francesco M, Primavera R, Romanelli D, Palomba R, Pereira R C, Catelani T, Celia C, Di Marzio L, Fresta M, Di Mascolo D, Decuzzi, P. Hierarchical microplates as drug depots with controlled geometry, rigidity, and therapeutic efficacy. *ACS Appl Mater Interfaces* **10**: 9280–9289 (2018)

[25] Dvir I, Abd-Rbo K, Segal D, Kandel LA, Kasem H. New experimental methodology to evaluate lubrication properties of synovial fluid containing worn tissue particles in osteoarthritis patients. *Friction* **11**(11): 2132–2141 (2023)

[26] Li X, Dai B, Guo J, Zheng L, Guo Q, Peng J, Xu J, Qing L. Nanoparticle–cartilage interaction: Pathology-based intra-articular drug delivery for osteoarthritis therapy. *Nano-Micro Lett* **13**: 149 (2021)

[27] Tevet O, Von-Huth P, Popovitz-Biro R, Rosentsveig R, Wagner H D, Tenne R. Friction mechanism of individual multilayered nanoparticles. *Proc Natl Acad Sci* **108**: 19901–19906 (2011)

[28] Shi J, Zhu X, Sun K, Fang L. Movement pattern of an ellipsoidal nanoparticle confined between solid surfaces: Theoretical model and molecular dynamics simulation. *Friction* **9**(5): 1098–1109 (2021)

[29] Li P P, Ji L, Li H X, Chen L, Liu X H, Zhou H D, Chen J M. Role of nanoparticles in achieving macroscale superlubricity of graphene/nano-SiO_2 particle composites. *Friction* **10**(9): 1305–1316 (2022)

[30] Fukubayashi T, Kurosawa H. The contact area and pressure distribution pattern of the knee: A study of normal and osteoarthrotic knee joints. *Acta Orthop Scand* **51**: 871–879 (1980)

[31] Schmidt T A, Gastelum N S, Nguyen Q T, Schumacher B L, Sah R L. Boundary lubrication of articular cartilage: Role of synovial fluid constituents. *Arthritis Rheumatol* **56**: 882–891 (2007)

[32] Link J M, Salinas E Y, Hu J C, Athanasiou K A. The tribology of cartilage: Mechanisms, experimental techniques, and relevance to translational tissue engineering. *Clin Biomech* **79**: 104880 (2020)

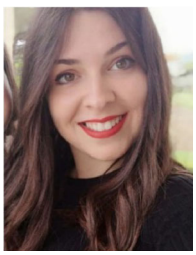

Agnese FRAGASSI. She is a Ph.D. student in the Laboratory of Nanotechnology for Precision Medicine at Istituto Italiano di Tecnologia (IIT), directed by prof. Paolo DECUZZI. Her research activities focus on the development of polymeric micro- and nano-particles for delivering different drugs (anti-inflammatory drugs and/or growth factors), in order to combine therapeutic activity and regenerative medicine. She joined IIT in March 2019 as master student for doing her thesis work and she achieved her MSc degree in November 2019 at the "G. D'Annunzio" of Chieti-Pescara discussing the thesis "Spherical polymeric nanoconstructs loaded with Docetaxel and Curcumin for the treatment of Neuroblastoma". In November 2020, she started her Ph.D. in sciences and technologies of chemistry and material at the University of Genoa, under the supervision of prof. DECUZZI. Her Ph.D. project is focused on the development microparticles made by biopolymers, as local drug delivery system for the treatment of osteoarthritis. From May 2022 to July 2022, she spent a period as visiting Ph.D. student at the Azrieli College of Engineering, in Jerusalem, under the supervision of prof. Haytam KASEM. She is currently a visiting Ph.D. student at Vanderbilt University (Biomedical engineering department) under the supervision of prof. Craig DUVALL.

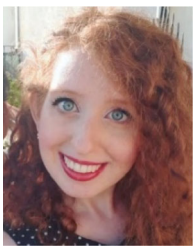

Antonietta GRECO. She obtained her master's degree, *cum laude*, in medical and pharmaceutical biotechnology, at University of Pavia in 2019. She obtained her Ph.D. in biomolecular science and biotechnology in 2023 at University School for Advanced Studies (IUSS) Pavia developing polymeric nanoplatforms for drug delivery. Currently, she is a postdoctoral fellow at Italian Institute of Technology. Her research activity includes the design and validation of nano/micro-delivery systems for various drugs.

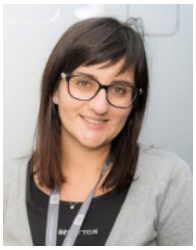

Martina DI FRANCESCO. She achieved her MSc degree in chemistry and pharmacology technology in 2013 at the "G. d'Annunzio" University of Chieti. In 2014, she started her Ph.D. in life sciences at University of Catanzaro. She has been a post doc in the Nanotechnology for Precision Medicine Research Laboratory at Italian Institute of Technology in Genoa from 2017 to 2022. She is now working for Pfizer Italy. Her research activities focused on the design and the development of polymeric micro- and nano-constructs for sustained drug delivery.

Luca CESERACCIU. He received his M.Sc. in materials engineering from University of Padova (Italy) in 2003 and his Ph.D. in materials science and metallurgical engineering from Technical University of Catalonia (Barcelona, Spain) in 2008. He joined Sandvik AB in 2008 as a competence engineer at Composite Materials Competence Centre in Sheffield (UK), then moved to Italian Institute of Technology in 2009 as a postdoctoral fellow in nanophysics. Since 2017, he is chief technician of the Materials Characterization Facility, where he manages the laboratory for mechanical characterization.

Aiman ABU AMMAR. He completed his pharmacy studies, MSc in medicinal chemistry, and Ph.D. in pharmaceutical sciences at The Hebrew University of Jerusalem. He then joined the nanoengineering group, Faculty of Mechanical Engineering, Technion. His current position is a senior lecturer in Department of Pharmaceutical Engineering at JCE. His research interests cover: localized drug delivery systems using nanotechnology (nanoparticles and nanofibers) for the treatment of various diseases, development of biomimetic mucoadhesive drug delivery systems; and microneedles for transdermal delivery.

Israel DVIR. He received his bachelor degree in mechanical engineering in 2022 from Azrieli College of Engineering Jerusalem (JCE), Israel. He joined the tribology and microstructure team headed by Prof. Haytam KASEM at JCE in 2020 as a research assistant student, and as a research engineer in 2022. His research areas cover the tribology of bionic microstructures and biotribology.

Thomas Lee MOORE. He completed his BSc in bioengineering at Clemson University (Clemson, SC–USA) with a focus on biomaterials, and continued in Bioengineering Department at Clemson in the Nanomedicine Lab of Prof. Frank ALEXIS. After completing his Ph.D., he joined the bionanomaterials group of Profs. Alke FINK and Barbara ROTHEN-RUTISHAUSER at Adolphe Merkle Institute (Fribourg, Switzerland) as a postdoctoral fellow in 2014. He is currently a Marie Skłodowska-Curie MINDED Research fellow at Italian Institute of Technology in Genoa. His research activity includes the study of the interface between biological systems and nanomaterials, application of machine learning towards formulation development in nanomedicine, and development nanoparticles to solve problems in the fields of drug delivery and bioengineering.

Haytam KASEM. He received his master's degree in mechanical engineering from the University of Haute Alsace in Mulhouse, France, in 2004. He received his Ph.D. degree in tribology of composite materials from the University of Orleans, France, in 2008. He joined the Tribology Laboratory at Technion, Israel, in 2012 and the Azrieli College of Engineering Jerusalem (JCE), Israel, in 2013. His current position is associate professor, head of the Department of Mechanical Engineering and head of the Tribology and Microstructure Laboratory at the JCE. His research areas cover the tribology of bionic microstructures, biotribology, mechano-chemical surface treatment, and tribology of friction brakes.

Paolo DECUZZI. He is a senior scientist and the founding director of the Laboratory of Nanotechnology for Precision Medicine at the Italian Institute of Technology in Genova–Italy. He earned his M.Sc. degree in mechanical engineering from the Polytechnic University of Bari (Italy) in 1997 and his Ph.D. degree in mechanical engineering from the University of Naples–Federico II (Italy) in 2001, with a thesis on friction and adhesion at the nanoscale. In 2002, he was nominated assistant professor of machine design at the Polytechnic University of Bari and, in 2005, he became associate professor in the School of Medicine of the University 'Magna Graecia' of Catanzaro. In October 2007, he joined The University of Texas Health Science Center in Houston as an associate professor of biomedical engineering. In October 2010, he moved to the Houston Methodist Hospital where he served as a professor of biomedical engineering till July 2015. There, he founded the Center for the Rational Design of Multifunctional Nanoconstructs, with the financial support of the Cancer Prevention and Research Center of Texas and the US National Cancer Institute; and served first as the co-chair of the Nanomedicine Department and then as the interim Chair of the Translational Imaging Department. In July 2014, he was awarded a European Research Council "Consolidator Grant" to design, synthesize and develop nanoconstructs for imaging and therapy in brain cancer. In July 2015, he joined the Italian Institute of Technology in Genova.